Melt Processing of Ethylene-Acrylic Acid Copolymer Composites Reinforced with Nanocellulose

Citation for the original published paper (version of record):

Venkatesh, A., Thunberg, J., Sjövold, K. et al (2020). Melt Processing of Ethylene-Acrylic Acid Copolymer Composites Reinforced with Nanocellulose. Polymer Engineering and Science, 60(5): 956-967. http://dx.doi.org/10.1002/pen.25351

Melt Processing of Ethylene-Acrylic Acid Copolymer Composit Reinforced with Nanocellulose

Venkatesh Abhijit,[1] **Thunberg Johannes**,[1] **Karin Sahlin-Sjövold**,[2] **Rigdahl Mikael**,[1] **Antal Boldizar**[1]
[1]*Department of Industrial and Materials Science, Chalmers University of Technology, SE-412 96, Gothenburg, Sweden*
[2]*Department of Chemistry and Chemical Engineering, Chalmers University of Technology, SE-412 96, Gothenburg, Sweden*

To investigate the impact of process design factors such as number of passes, screw design and screw type, a poly(ethylene-*co*-acrylic acid) and a masterbatch containing 40 vol% nanocellulose were compounded using a twin-screw extruder with two different screw configurations. The 20 vol% composite pellets obtained, containing nanocellulose of different morphologies, cellulose nanofibrils and cellulose nanocrystals, were re-extruded several times to study the effect of re-extrusion. The compounded pellets were extruded into films using a single-screw extruder. These films contained aggregates of the nanocellulose material, which was reduced in size upon re-extrusion leading to an improvement in properties of the composites. With the best combination of process factors, the Young's modulus and stress at break of the composites increased by factors of 10 and 1.6, respectively. The presence of a strong network of the cellulosic entities was observed qualitatively using melt rheology upon re-extrusion. Re-extrusion had a negligible effect on the crystallinity of the composites. POLYM. ENG. SCI., 60:956–967, 2020. © 2020 The Authors. ***Polymer Engineering & Science*** **published by Wiley Periodicals, Inc. on behalf of Society of Plastics Engineers.**

INTRODUCTION

Cellulose has been used as a reinforcement/filler in the plastics industry for decades and with the development and commercial availability of nanocellulose the possibilities of utilizing this material as a reinforcement in polymers have been rekindled [1]. The good specific mechanical properties (stiffness and strength), large surface area, and high aspect ratio of this nanoscale cellulose have made it a viable option in composite applications [2, 3]. However, to realize the potential of nanocellulose as a reinforcement in thermoplastics, it is necessary to solve the problems involved in the melt processing of these composites. Nanocellulose, due to its hydrophilic nature, tends to give problems during melt processing with a hydrophobic thermoplastic matrix. This incompatibility can lead to the formation of cellulose aggregates, which lead to poorly dispersed, nonuniform thermoplastic composites. The adhesion between the matrix and the reinforcement is also affected by this incompatibility, leading to poor mechanical properties due to inefficient stress transfer. The ways to improve the compatibility of the reinforcing elements are by the addition of compatibilizers or surface modification of these elements. In the present case, interest leans toward the use of compatibilizers due to the ease of scalability. This approach makes it necessary to explore the processability of these nanocomposites using industrial melt processing technologies such as compression molding, extrusion, and injection molding instead of laboratory-scale processing. The work done on continuous extrusion as summarized in the review by Oksman et al. [3] is limited with only a few succeeding at showing promising results in the recent years [3–5]. Nevertheless, there is, to our knowledge, no work which explores the effect of processing parameters, the effect of screw selection during extrusion and the effect of number of passes (re-extrusion) on the morphology, appearance, melt rheology and mechanical properties of these composites.

In the present work, a grade of poly(ethylene-acrylic acid) copolymer, with a relatively high content of acrylic acid, has been mixed with nanocellulose to obtain a 40 vol% masterbatch as described previously [6]. The poly(ethylene-*co*-acrylic acid), which have been used in the packaging industry, has shown to have good compatibility and adhesion with cellulose due to the presence of the acrylic acid groups [6, 7].This masterbatch was compounded with another grade of poly(ethylene-acrylic acid) copolymer with a lower content of acrylic acid. Composites containing 20 vol% dry content of nanocellulose were processed with variables ranging from screw configuration during compounding and shaping to the effect of reinforcement morphology on the final composite. To better understand the effects of these processing variables on the reinforcing ability of the nanocellulose, the thermal, rheological, and mechanical properties of the composites were studied.

METHODS

Materials

The cellulose nanofibril (CNF) suspension derived from spruce sulfite pulp used in this study was kindly provided by Borregaard A/S, Norway. It had a solids content of 2 wt%. The wood polymer content of the CNF, determined by monosaccharide carbohydrate analysis, showed a Klason lignin content of 3.2 wt%, hemicellulose content of 2.8 wt% with the rest being cellulose. The sulfuric-acid-hydrolyzed cellulose nanocrystals (CNC) from Celluforce, Canada, were received as a spray-dried powder which was dispersible in water.

Two grades of poly(ethylene-acrylic acid) copolymer containing 15% acrylic acid (EAA15) and 7% acrylic acid (EAA7) were obtained from BIM Kemi AB, Sweden and Dow Chemical Company, Sweden, respectively. The EAA15, an aqueous dispersion neutralized to its ionomer form using NaOH, had a solids

Correspondence to: V. Abhijit; e-mail: abhijit.venkatesh@chalmers.se
Contract grant sponsor: Wallenberg Wood Science Centre. contract grant sponsor: Knut and Alice Wallenberg Foundation. contract grant sponsor: Swedish Foundation for Strategic Research.
DOI 10.1002/pen.25351
Published online in Wiley Online Library (wileyonlinelibrary.com).

content of 20 wt%, a density of 0.994 g/cm^3, a melting point of 88°C and a melt flow rate of 36 g/10 min (ISO 1133, 190°C, 2.16 kg), according to the supplier. The EAA7 grade (in the form of pellets) is denoted Primacor 3540 and had a number average molecular weight (M_n) of 16,100 g/mol, a melt flow rate (MFR, 190°C/2.16 kg, ISO 1133) of 8 g/10 min and a density of 0.932 g/cm^3 according to the supplier.

Microscopy and Visual Appearance

The dimensions of the CNC were evaluated from a 10-ppm dried dispersion using atomic force microscopy (AFM) in the tapping mode (Nanoscope IIIa with a Micro Masch silicon cantilever NSC 15 with a type G scanner, Digital Instruments Inc.). The morphology of the dried CNF suspension and the cross section of cryo-fractured composites were assessed by scanning electron microscopy (SEM) using LEO ULTRA 55 FEGSEM. The samples were gold sputtered for 80 s at 10 mA to obtain a 10 nm thick coating of gold. The presence of aggregates in the extruded films was analyzed using a stereo-microscope (SteREO Discovery V20 from Carl Zeiss, Germany). Images from three different regions of the extruded film were studied.

The discoloration of the nanocellulose composite was assessed visually.

ζ-Potential

The CNC dispersion was diluted to a concentration of 0.05 wt % before ion exchange. The ζ-potential of the CNC was measured at 25°C using a Zetasizer Nano ZS (Malvern Instruments, UK) based on the Laser Doppler Velocimetry technique. The light source was a 50-mW diode-pumped solid-state laser with a wavelength of 532 nm, and a DTS1070 disposable folded capillary cell was used. The analyses were performed in triplicate and before each run, the sample was stabilized for 120 s.

Production of Composites

The masterbatch-containing CNF and EAA15 was prepared by a method similar to that described in an earlier study where the EAA15 dispersion was mixed with the CNF suspension in excess of water [6]. The CNF-based masterbatch, having a solids content of 3–4 wt%, was mixed using a L&W pulp disintegrator (Lorentzen & Wettre, Sweden) for 60,000 revolutions at 2900 rpm. For the preparation of the CNC-based masterbatch, the Celluforce powder was first dispersed in water using a magnetic stirrer and then exposed to high shear rates using an Ultra Turrax at 14,000 rpm for 8 min to obtain a CNC dispersion with a solids content of 4 wt%. The CNC dispersion was then mixed with EAA15 as described in the literature [6].

The masterbatch containing 40 vol.% nanocellulose, either CNF or CNC, was dried at room temperature and then dried for 3 days at 40°C in a dehumidifying dryer (Moretto, Italy). The final water content in the masterbatch was about 2 wt%. The masterbatch was then compounded with EAA7 using a twin-screw extruder (TSE) using two different screw configurations (S1 and S2), see Fig. 1, at 100 rpm. The material was compounded three times in the TSE before being shaped in the single-screw extruder (SSE). In Fig. 1, the screw element designation were as follows: the forward conveying screw elements were designated as *C* (*Pitch/Length*), the reverse conveying element was designated as *C (Pitch/Length) (L)*, the forward kneading elements were designated by *K* (*Staggering angle/Number of disks/Length*) and the neutral kneading elements were designated as *K* (*Staggering angle/Number of disks/Length*) *(N)*.

The screw configurations were chosen in order to break up the aggregates during the melt processing operation, mainly by making use of an extended kneading section in the screws. The S1 screw configuration gave a residence time between 7 and 8 min, and the residence time with the S2 screw configuration was 4–5 min. The longer residence time with the S1 screw configuration was due to the presence of a reverse-conveying screw element, C 10/10 (L), which restricted the forward melt flow. The residence time was measured in two ways; in the first method, the barrel was filled with EAA7 (matrix) and then the nanocellulose masterbatch was fed in through the hopper to prepare the composite. The feed rates of EAA7 and the master-batch was adjusted to obtain 20 vol% in the final composite. Here, the time taken for the appearance of the first trace of browning of the melt or aggregates at the exit of the die was noted. In the second method, a colored pellet was added into the hopper while the EAA7 and masterbatch were being simultaneously fed into the system and the time taken for the first trace of the color to appear at the die exit was noted.

The TSE used was a co-rotating twin-screw extruder, Werner & Pfleiderer ZSK 30 M9/2 (Stuttgart, Germany), having a, D_a/D_i = 1.44, screw diameter of 30 mm, and a screw length of 966 mm. The TSE had five heating zones along the cylinder and one heating zone at the end for the die. The temperature profile from the hopper to the die was 90–130–140–140–140–150°C. The final nanocellulose content in the composite was adjusted to 20 vol% by adding the EAA7. The average throughput and the energy input of the TSE were approximately 1.3 kg/h and 14,256 kJ/h, respectively.

The final shaping of the compounded pellets was performed using a Brabender SSE, Brabender OHG, Duisburg, Germany, with a screw diameter of 19 mm and a screw length of 25*D* with three individually controlled temperature zones and a temperature-controlled flat die with a width of 100 mm and slit height of 1 mm. In order to study the effect of the type of barrier flank screw on the shaping, a Maddock type barrier screw (M) with a compression ratio of 2:1 and a Maillefer type barrier screw (B) having a compression ratio of 2.5:1 with a Saxton type distributive mixing profile, both provided by Brabender, were used. The temperature profile from the hopper to the die was 90–130–140–150°C with a screw rotation rate of 30 rpm. The average throughput and the energy input of the SSE were approximately 1 kg/h and 940 kJ/h, respectively. The entire composite production method is described schematically in Fig. 2.

The 20 vol% composites were given denotations based on the reinforcement used, the number of passes through the TSE, the screw design during compounding and the screw type used during shaping. For example, the sample-containing CNF, which has been passed through the TSE twice, compounded using the S1 screw design and shaped with the Maddock type barrier screw were denoted "*CNF-2P-S1-M*."

Mechanical Properties

The Young's modulus (E), stress at break (σ_b), and elongation at break (ε_b) were evaluated in accordance with ISO 527-3. Samples were cut into dumbbell shapes having a width of 4 mm and a thickness of approximately 1 mm and were conditioned for at

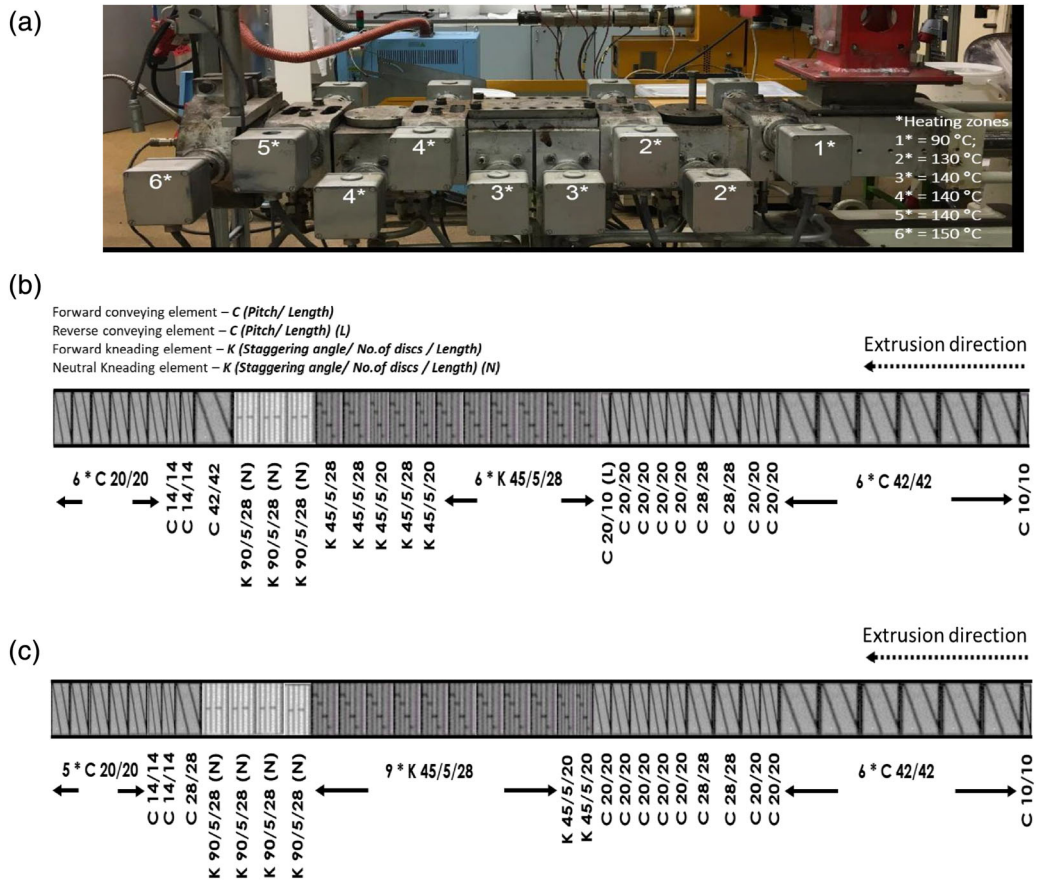

FIG. 1 Image of the twin-screw extruder with the heating sections and a schematic representation of the screw for the twin-screw extruder consisting of (a) S1 and (b) S2, screw configurations. [Color figure can be viewed at wileyonlinelibrary.com]

least 2 days at $23 \pm 2°C$ and $50 \pm 5\%$ relative humidity (RH) prior to testing. The tensile measurements were performed in a conditioned room with a Zwick Z1/Roell with a grip separation of 40 mm and a cross head speed of 6 mm/min. A Zwick μEye UI 1540 M video extensometer was used, with an initial gauge length of 20 mm. A load of 0.1 N was applied before measurement. The standard deviations were obtained from more than six successful replicates of each sample.

Melt Rheology

Small-amplitude oscillatory shear tests (SAOS) were performed on the extruded samples at 150 °C using an Anton Paar MCR 702 rheometer (Graz, Austria) with parallel plate geometry (15 mm plate diameter). The disk-shaped samples were compression molded at 140°C and 50 MPa to a thickness of 2 mm. The plate gap was set at 1.9 mm by gradually squeezing the sample. The composites were found to be stable at 150°C for a period of over 100 min. Hence, thermal degradation during the rheological measurements was considered to be negligible.

In SAOS experiments, the linear viscoelastic region was first assessed using a strain sweep from 1 to 100% at a constant angular frequency of 1 s^{-1}. In addition to the strain sweeps, angular frequency sweeps in the range of 0.08–200 s^{-1} were performed at low strain amplitudes of 0.2%. In most cases, the experiments were repeated twice (using different specimens).

Steady shear viscosity measurements were also performed on the composites using the parallel-plate fixtures at shear rates between 0.1 and 10 s^{-1}. The plate gap and the temperature were the same as those stated above.

Differential Scanning Calorimetry

Differential scanning calorimetry (DSC) using a Perkin-Elmer DSC7 was employed to assess the thermal transitions and the crystallinity of the composite materials. The endotherms were recorded when the temperature was raised from 20 to 180°C at a rate of 10°C/min, that is, no second temperature scan was used. The crystallinity (X_c) was evaluated as

$$X_c = \frac{\Delta H_c}{w_{EAA}\Delta H_o} \quad (1)$$

where ΔH_c is the specific heat of fusion of the composite, w_{EAA} the weight fraction of EAA, and ΔH_o is the specific heat of fusion for 100% crystalline polyethylene; 286.19 J/g [8].

Thermal Gravimetric Analysis

Thermal gravimetric analysis (TGA) was employed to assess the thermal stability of the extruded composites using a TGA/DSC 3 + Star system (Mettler Toledo, Switzerland). A 5 °C/min heating rate was used to heat an approximately

 DOI 10.1002/pen

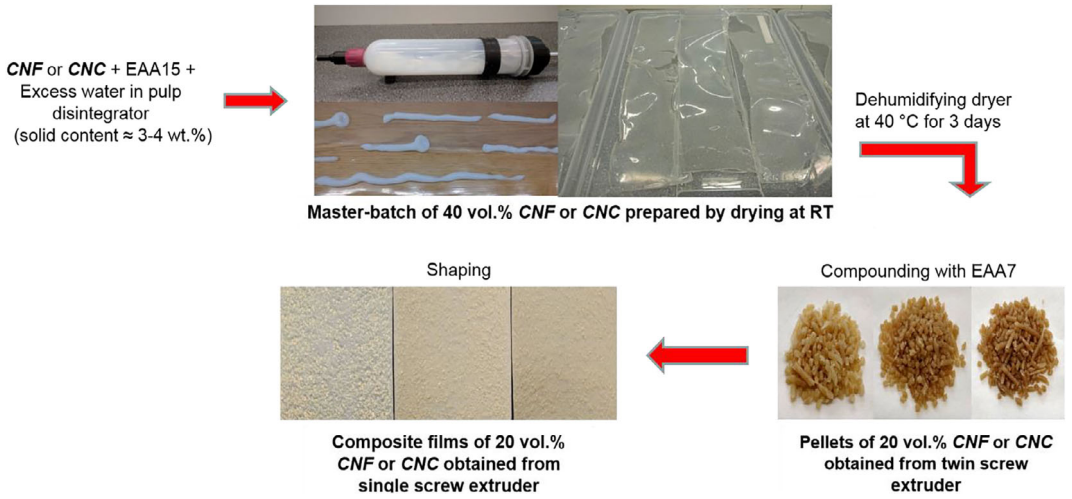

FIG. 2 Schematic representation of the preparation of 20 vol% nanocellulose-reinforced composite. [Color figure can be viewed at wileyonlinelibrary.com]

5 mg sample from 25 to 500°C under a nitrogen at a flow rate of 20 mL/min.

RESULTS AND DISCUSSION

Characterization of the Reinforcement

The CNF used exhibited a wide distribution of fiber dimensions ranging from fibers to micro- and nano-fibrils, see Fig. 3a [6]. The CNC, which was characterized by AFM, see Fig. 3(b), had an average length of 301 ± 110 nm and a diameter of 6 ± 3 nm. The ζ-potential measurements, which were used to characterize the surface charge of the dispersed CNC, gave a value of −69.7 (±2.0) mV, which indicates a stable CNC dispersion.

Microscopy and Visual Appearance of the Melt-Processed Composites

Compounding. The masterbatch containing 40 vol% nanocellulose and 60 vol% EAA15 was compounded with EAA7 using the TSE at the temperatures given in the experimental section. During the compounding step, the material was re-extruded three times through the TSE resulting in a discoloration which became more pronounced as the number of passes through the extruder increased, see Fig. 4.

The degradation was more evident for pellets prepared with the S1 screw configuration which yielded an average residence time between 7 and 8 min. This more pronounced discoloration could be associated with the longer exposure time due to the presence of a reverse conveying element (left-hand screw in Fig. 1a), which limits the forward movement of the solid pellets and allows only the melt to flow forward. The CNF-reinforced pellets compounded with the S2 screw configuration exhibited a moderate amount of discoloration due to the shorter residence time, 4–5 min, in the barrel. However, in the case of the CNC-reinforced pellets, even though the residence time was short, the degradation increased with the number of passes with the S2 screw configuration, due to the limited thermal stability of the CNC (to be discussed later).

Shaping. The CNF-containing pellets obtained from this compounding process were converted into films using the Maddock type barrier screw and the Maillefer type barrier screw. The extruded films contained aggregates, as shown in

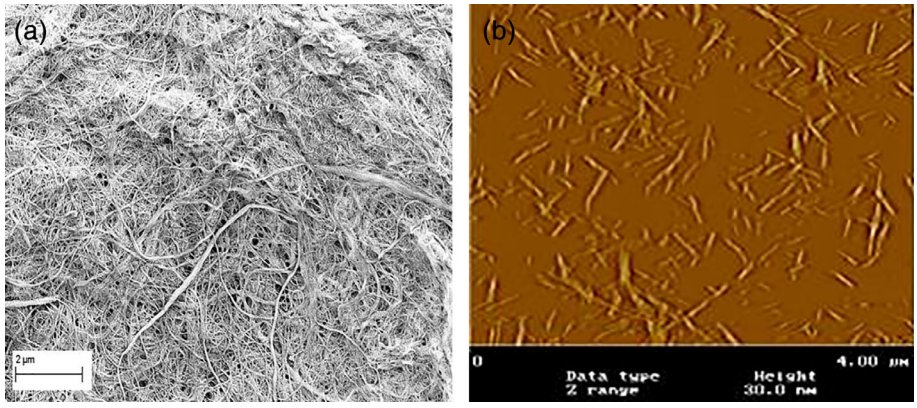

FIG. 3 (a) Scanning electron micrograph and (b) atomic force micrograph of dried cellulose nanofibrils and cellulose nanocrystals, respectively. [Color figure can be viewed at wileyonlinelibrary.com]

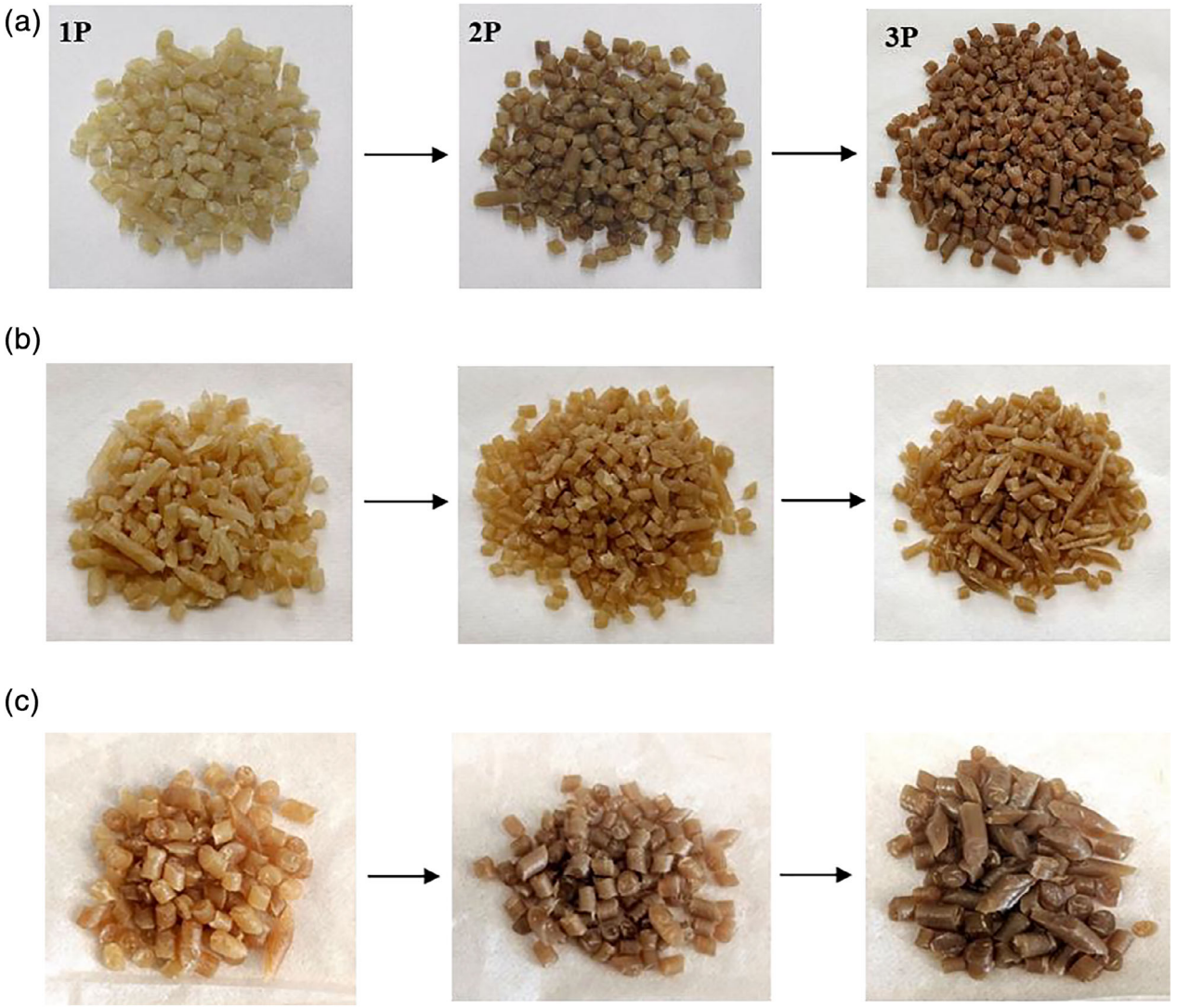

FIG. 4 Photographs of 20 vol% (a, b) CNF and (c) CNC-reinforced pellets compounded using (a) S1 and (b, c) S2 screw configuration, in TSE. The images in the left-hand column show a single pass sample (1P) and the images in the right-hand column show a three-pass sample (3P). [Color figure can be viewed at wileyonlinelibrary.com]

Figs. 5 and 6, whose size was reduced with increasing number of passes. Figure 5 shows the effect of screw design on the morphology of the CNF-containing films. The S1 screw configuration, with the longest residence time, was more effective in reducing the size of the aggregates with increasing number of passes than the S2 screw configuration, see Fig. 5b. The SEM images for the samples produced with the S2 screw design showed the presence of a large number of voids even after three passes. However, the discoloration of the samples was less pronounced with the S2 screw configuration, probably due to the shorter residence time.

Figures 5a and 6a show the effect of screw type during film-forming (with the SSE) on the morphology of the CNF-containing film morphology. As in the previous case, the size of the aggregate was reduced with increasing number of passes. The Maddock-type barrier screw seemed to be more efficient in reducing the size of the aggregates, probably due to high shear regions in the screw. The two-pass and three-pass samples showed the presence of a fibrillar structure, which could be related to the ability of the nanofibrils to form networks, see the SEM micrographs in Fig. 6a.

In Figs. 5b and 6b, the effect of the reinforcement morphology (CNF or CNC) on the film is shown. As before, the aggregate size decreased with increasing number of passes. The CNC samples, Fig. 6b, exhibited an aggregate size smaller than that in the CNF-based samples, owing to the rod like, morphology of the reinforcements (see Fig. 3b). However, the discoloration of the samples was less with the S2 screw configuration for CNF-reinforced samples than for the CNC-reinforced composites despite the shorter residence time. This can be related to the lower thermal stability of sulfuric-acid-hydrolyzed CNC due to the presence of sulphate ester groups [9, 10].

Mechanical Properties of the Composites

The EAA7 matrix exhibited a high ductility with a failure strain of approximately 420% which was significantly reduced with the addition of nanocellulose. The 20 vol% reinforced

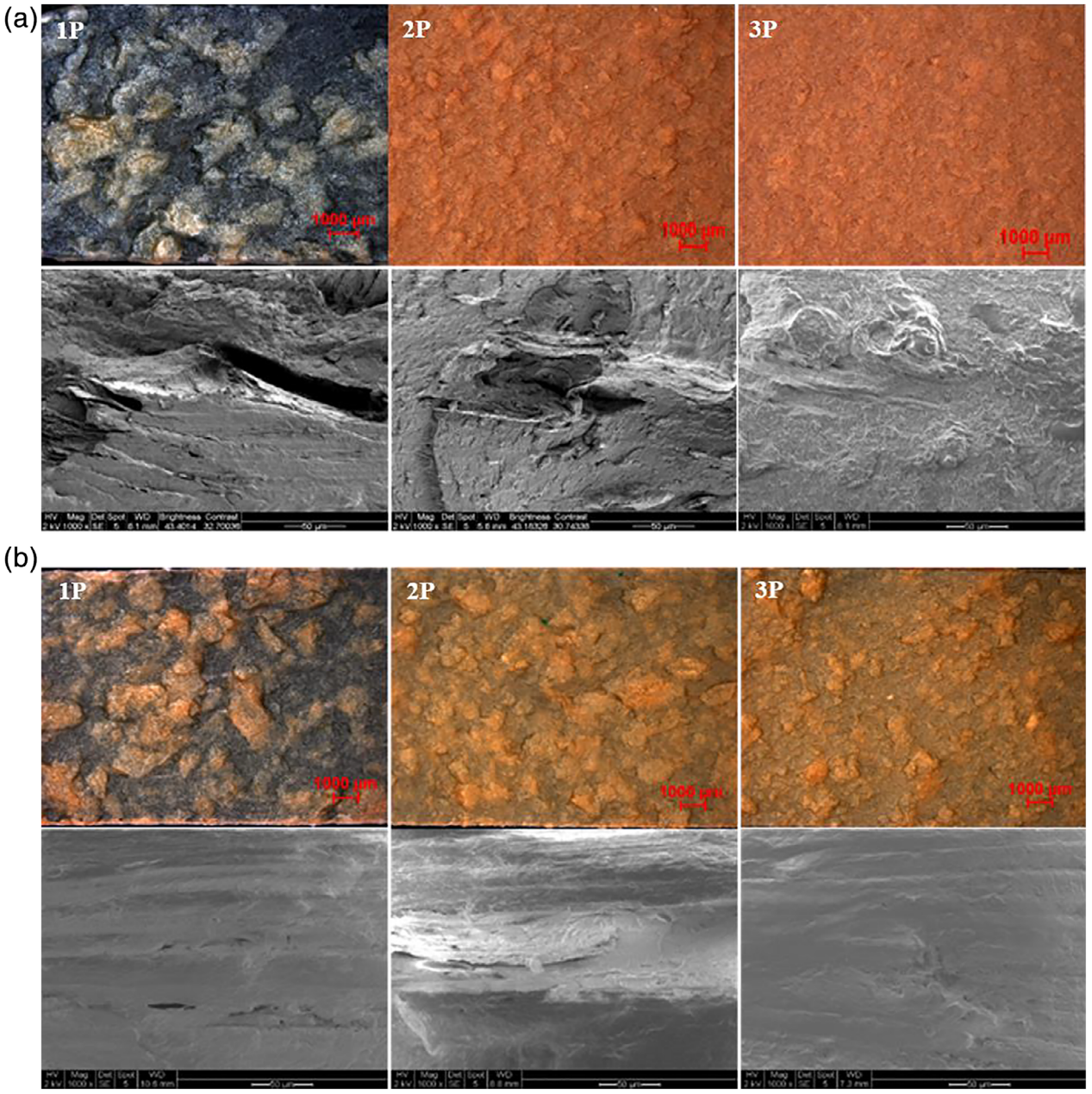

FIG. 5 Stereo-micrographs (with color) and SEM images (greyscale, 1,000×, 50 µm) of 20 vol% CNF-reinforced films compounded using (a) S1 and (b) S2 screw configuration, respectively, and shaped using the Maddock-type barrier screw. [Color figure can be viewed at wileyonlinelibrary.com]

composites were stiffer with a modulus (E) increasing by a factor of up to 4.8.

The mechanical properties (modulus, strength at break, and elongation at break) were improved with an increasing number of passes and the three-pass composites had the best properties among the sample series, see Fig. 7. For the 20 vol% CNF-reinforced composites processed using the S1 screw configuration, the tensile modulus (E), the stress at break (σ_b), and the elongation at break (ε_b) increased from 550 MPa, 10.3 MPa, and 6.7%, respectively, after one pass (CNF-1P-S1-M) to 1,340 MPa, 27.7 MPa and 10.4%, respectively, after the third pass (CNF-3P-S1-M). On the other hand, the samples compounded using the S2 screw configuration showed relatively lower values with a tensile modulus (E), stress at break (σ_b), and elongation at break (ε_b) of 470 MPa, 10.6 MPa, and 10.2% respectively, after one pass (CNF-1P-S2-M), and 510 MPa, 15 MPa, and 12.5%, respectively, after the third pass (CNF-3P-S2-M). The stress at break (σ_b) of the samples compounded with the S2 screw configuration was lower than that of the matrix. The longer residence time of the S1 screw configuration gave a better mixing and break down of aggregates and this increased the melt homogeneity and improved the network strength, which led to higher E-and σ_b-values, as shown in Fig. 7.

Figure 8 shows the effect of screw type during shaping on the mechanical performance of the composites (for the S1

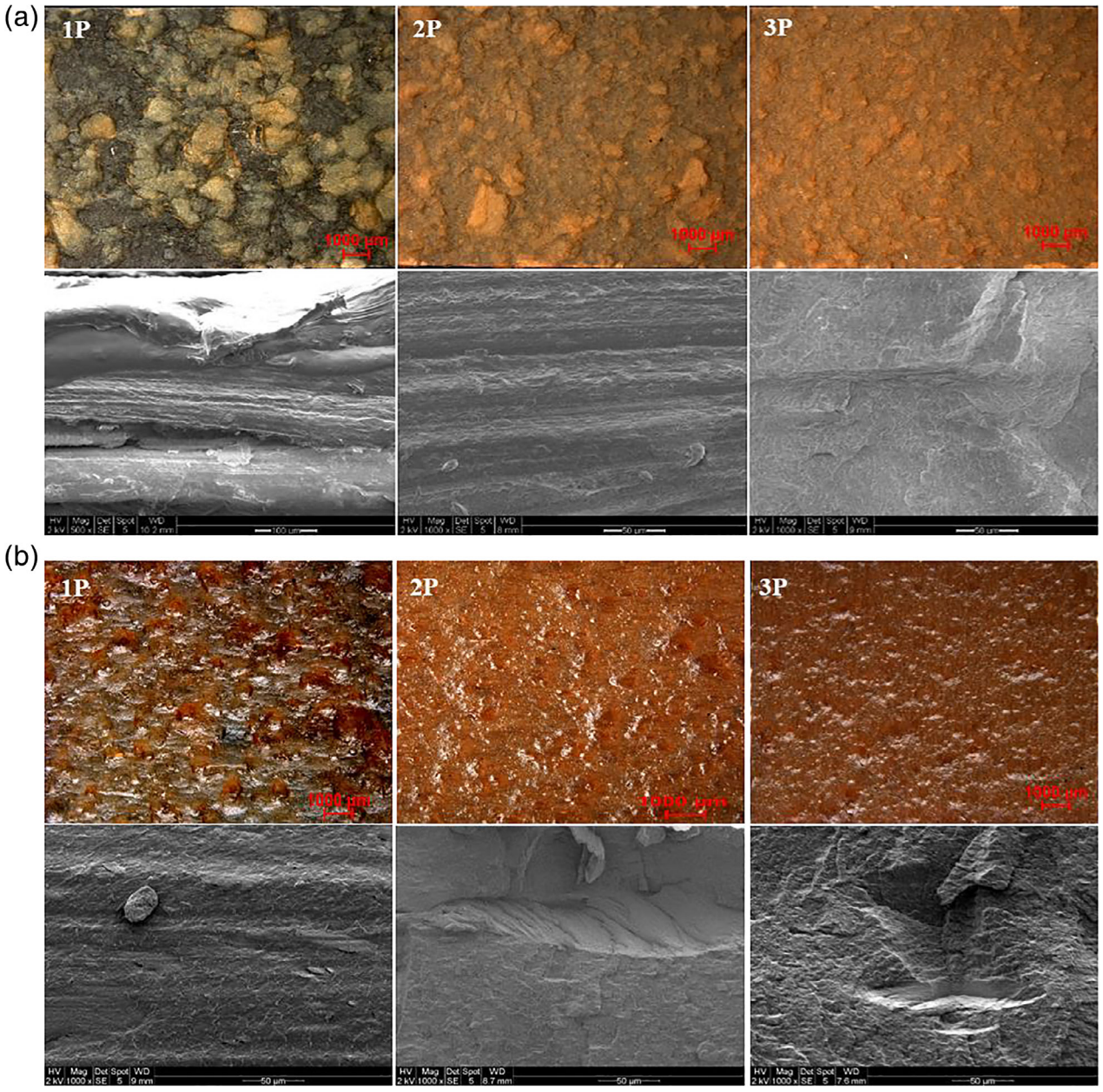

FIG. 6 Stereo-micrographs (with color) and SEM images (greyscale) of 20 vol% (a) CNF and (b) CNC-reinforced films compounded using (a) S1 and (b) S2 screw configurations and shaped using the Maillefer barrier screw. [Color figure can be viewed at wileyonlinelibrary.com]

configuration). Here, the mechanical properties increased, as expected, with increasing number of passes and the three-pass composites exhibited the most improved properties in the sample series. The 20 vol% CNF-reinforced composites formed using the Maillefer-type barrier screw exhibited the best properties with the tensile modulus (E), stress at break (σ_b), and elongation at break (ε_b) increasing from 773 MPa, 12.6 MPa, and 6.7%, respectively, in one pass (CNF-1P-S1-B) to 1,530 MPa, 30.4 MPa, and 9.6%, respectively, after the third pass (CNF-3P-S1-M). The combination of S1 screw configuration during compounding and the Maillefer-type barrier screw during shaping gave the best results among all the extruded composites, probably because of the better dispersive and distributive mixing that was achieved with this combination.

The impact of reinforcement morphology on the mechanical properties is evident as shown in Fig. 9. The CNC-containing composites showed an improvement in tensile modulus (E) and elongation at break, ε_b, with increasing number of passes, but, the σ_b values were lower than that of the matrix. The tensile modulus (E) modulus was greater than that of the matrix and increased moderately with increasing number of passes. The elongation at break, ε_b, of the CNC sample also increased with increasing number of passes, from 47% after one pass to 62% after the third pass, suggesting that it might be possible to explore higher CNC loading in the

 DOI 10.1002/pen

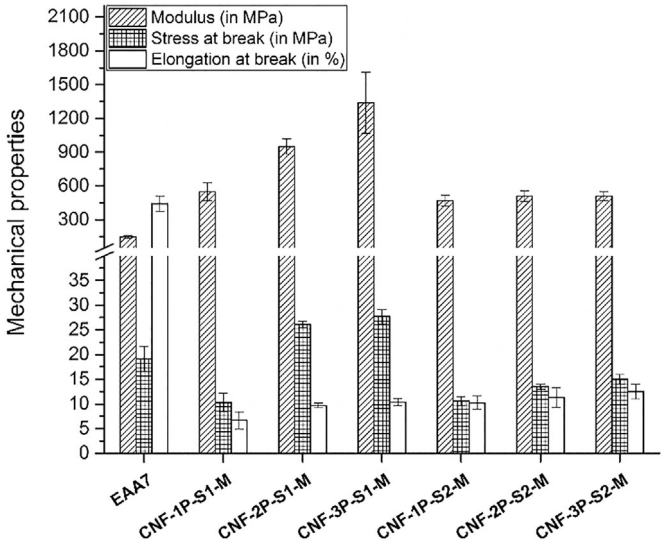

FIG. 7 The mechanical properties of CNF-reinforced samples compounded using different screw designs (S1 and S2) and shaped with the Maddock-type barrier screw.

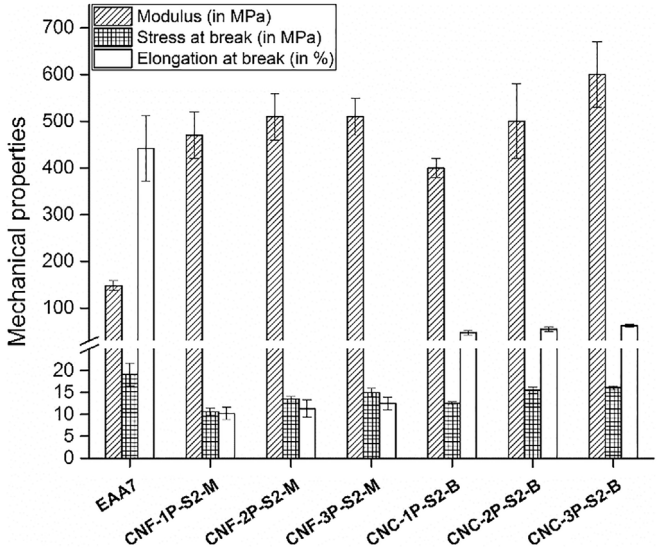

FIG. 9 The mechanical properties of CNF- and CNC-reinforced samples compounded using the S2 screw design and shaped with the Maddock type barrier screw (CNF) and Maillefer barrier screw (CNC).

composite in order to acquire a stronger network similar to that of the CNF-based composites. As expected, the extent of reinforcement of the CNC was lower than that of the CNF-composites, with a similar loading content, except for the *CNF-S2-M* series.

From all the above results, it is safe to say that, the discoloration/degradation of the composites had minimal effect on the mechanical properties and it was in fact the screw configuration with the longest residence time (S1), which yielded the largest improvements in mechanical properties. It is clear from the mechanical properties that the re-extrusion actually improved the mechanical properties of the samples and did not reduce their strength as suggested otherwise [11].

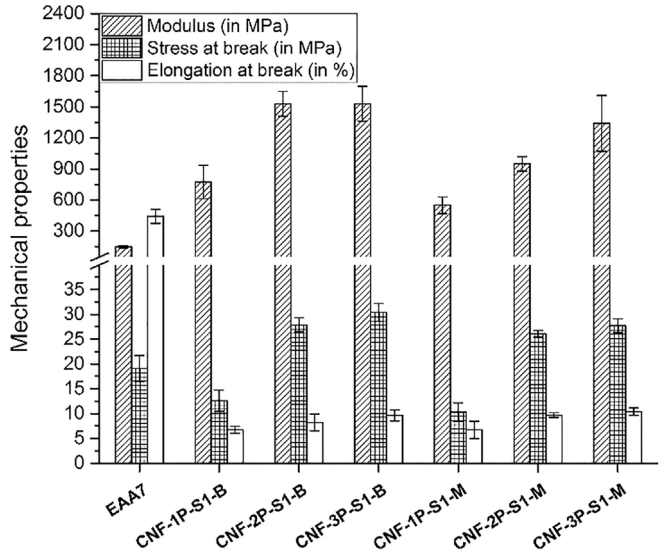

FIG. 8 The mechanical properties of CNF-reinforced samples compounded using the S1 screw design and shaped with different barrier screws (Maddock or Maillefer barrier screw).

Melt Rheology

The rheological properties of the composites in the molten state were characterized by SAOS and steady shear rate experiments. The composites had a reinforcement content of 20 vol%. The strain amplitude experiments on all the samples led to a strain amplitude value of 0.2% being adopted for all the extruded samples for the frequency sweep test. In Figs. 10–12, it is important to note that the two-pass sample data have been omitted due to their overlap with the results of the three-pass samples.

Small amplitude oscillatory shear. The results of the strain sweep experiments and the frequency sweep tests are summarized in Figs. 10a, 11a and 10b, 11b. In general, the shear storage modulus (G') of the samples increased in general with increasing number of passes through the TSE, regardless of the screw design or reinforcement morphology. In all cases, the reinforced samples exhibited a higher storage modulus (G') than the matrix material, and the increase in storage modulus was greater, by an order of magnitude, for the materials compounded using the S1 screw design, see Figs. 10a and 11a. The effect of screw type during shaping was only visible in the first pass sample, the Maillefer barrier screw producing a higher G' than the Maddock-type barrier screw, whereas the curves for the second- and third-pass samples were virtually the same, see Fig. 10a. The CNF-containing composites had a higher storage modulus than the CNC-containing samples, whose third-pass sample showed a G' similar to that of the one-pass CNF-containing samples compounded using the S2 screw configuration, see Fig. 10a. In all cases, the span of the linear viscoelastic region (LVR) decreased with increasing number of passes.

The increase in G' and decrease in the span of the LVR can be related to the breakdown of the aggregates which increases with increasing number of passes, see Figs. 5 and 6. This breakdown increases the surface area of the cellulose phase in the samples and leads to a stronger cellulosic network which could result in longer relaxation times, consistent with

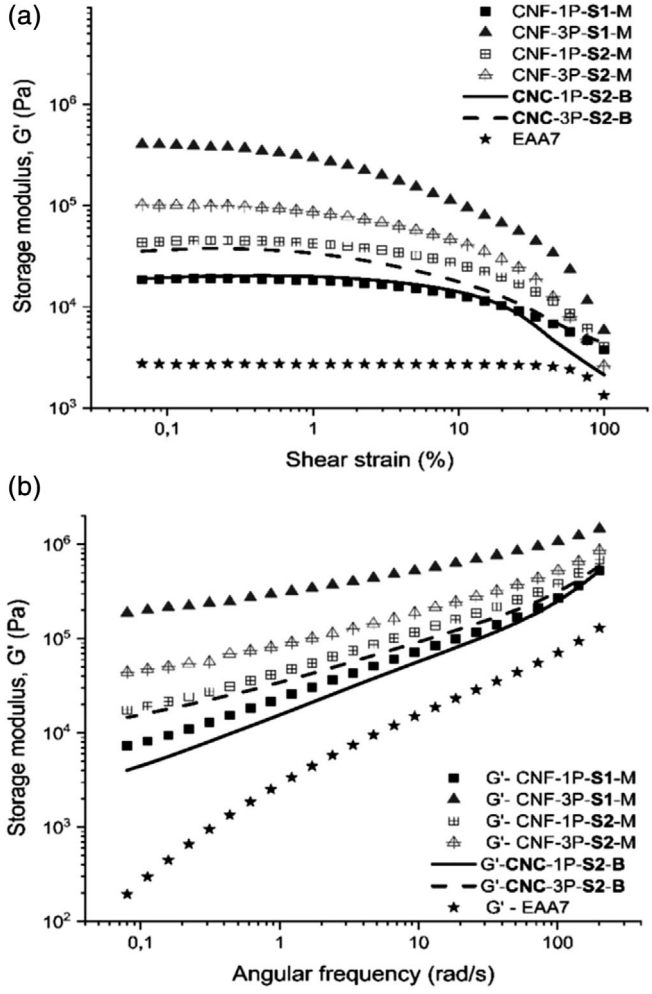

FIG. 10 The storage (*G'*) moduli as functions of (a) the shear strain amplitude and (b) angular frequency for CNF- (symbols) and CNC- (lines) reinforced samples compounded using S1 (solid symbols) or S2 (open symbols and lines) screw configurations and shaped using either the Maddock type (symbols) or the Maillefer barrier screw (lines).

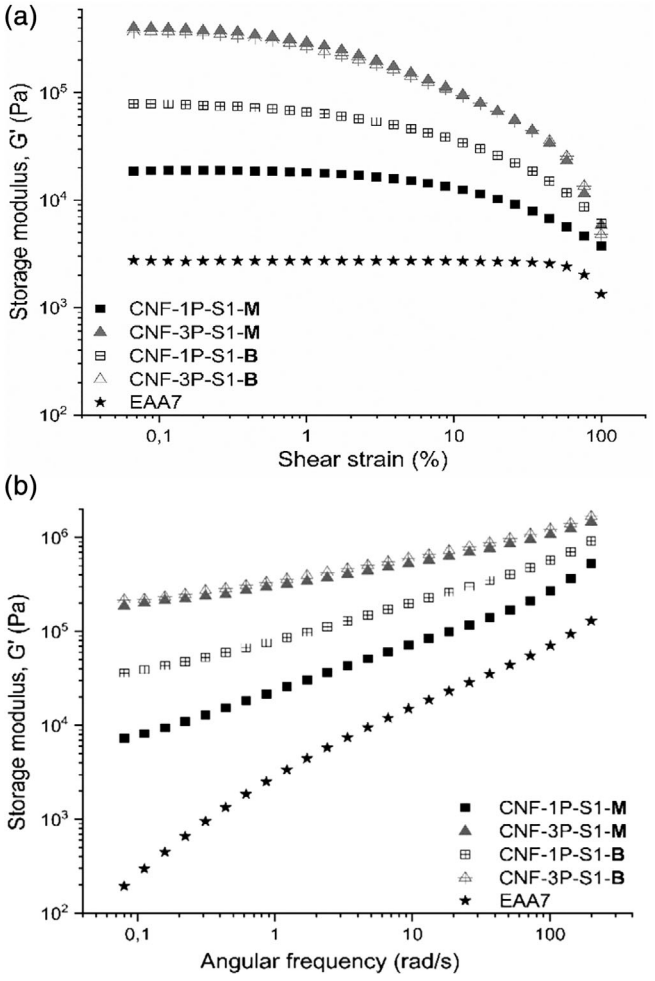

FIG. 11 The storage (*G'*) and loss moduli (*G''*) as functions of (a) the shear strain amplitude and (b) angular frequency for CNF-reinforced samples compounded using S1 screw configurations and shaped using either the Maddock-type (solid symbols) or Maillefer barrier screw (open symbols).

percolated nanocellulose-reinforced composites [12, 13]. The similarity between the two-pass and three-pass sample curves suggests a limit up to which the properties of the composites can be improved through processing.

Figures 10b and 11b show the variation in storage moduli (*G'*) with respect to angular frequency (ω). Here, the values of *G'* after two and three passes were higher than the *G*' value of the respective sample, after one pass. This was particularly evident at low frequencies. At lower frequencies, the slope of the *G'* in the frequency sweep, tends to decrease with increasing number of passes, suggesting an improved network and a more elastic melt behavior.

The value of *G'* stabilized after two passes, that is, the two- and the three-pass samples followed a similar trend with little difference between them. Apart from the increase in *G'*, the reinforced samples also exhibited a lower slope at lower frequencies (approaching a plateau level) which increased with the number of passes and stabilized after two passes. Figure 11b reveals that the materials compounded using the S1 screw configuration showed a large increase in *G'*, whereas the S2 screw configuration samples showed little difference between *G'* after each pass. The reduction in slope in the low-frequency region was more evident with the S1 screw configuration. Figure 10b shows the effect of screw type during shaping (which was evident for the first-pass sample), where the Maillefer barrier screw had a stronger effect than the Maddock-type barrier screw, while the second- and third-pass samples exhibited similar behavior, and both the Maddock-type barrier screw and the Maillefer barrier screw exhibited a similar reduction in the slope.

The CNF-containing composites had a higher *G'* than the CNC-reinforced samples, whose third pass sample had *G'* values similar to that of the one-pass CNF-containing samples, see Fig. 10b. As expected, the CNF-containing samples displayed a greater reduction in slope. The increase in *G'* can, as mentioned previously, be related to aggregate breakdown, whereas the lower slope at lower frequencies indicates a pseudo-solid behavior observed in systems with a percolated network [12, 14]. The presence of a stronger network was also evident from the pressure transducer readings at the die during shaping which recorded higher pressure values of 58 bar and 75 bar for the two-pass and three-pass CNF-containing samples, respectively. The network is strengthened with increasing number of passes, which could be due to the increased surface area resulting from the breakdown of aggregates.

DOI 10.1002/pen

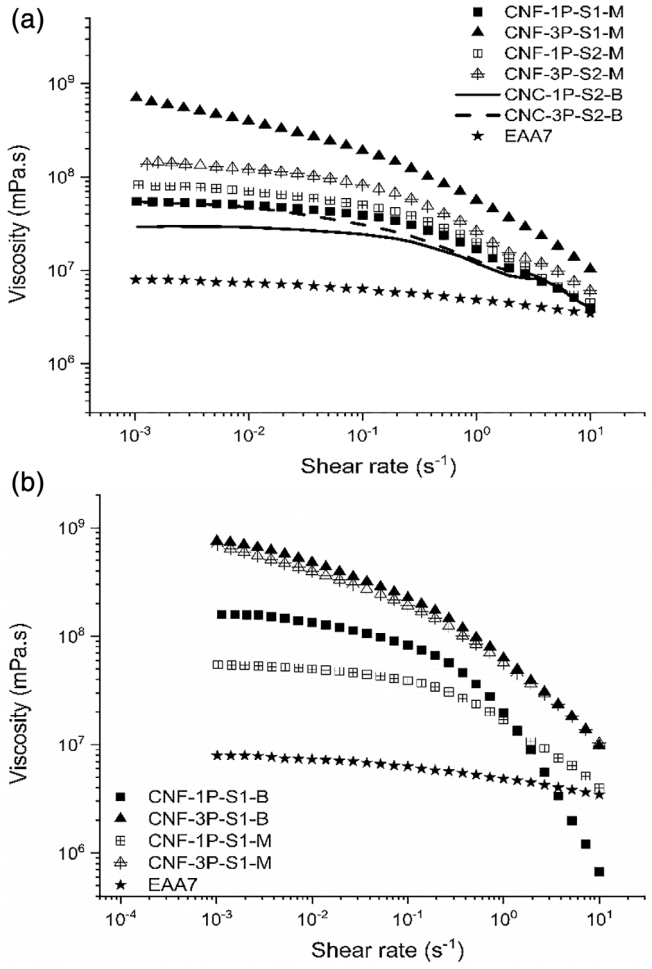

FIG. 12 The viscosity (η) and loss moduli ($\dot{\gamma}$) for (a) CNF- (symbols) and CNC-(lines) containing composites compounded using S1 (solid symbols) or S2 (open symbols and lines) screw configurations and shaped using either the Maddock type (symbols) or the Maillefer barrier screw (lines) (b) CNF-containing composites compounded with S1 screw configuration and shaped using either the Maddock type (solid symbols) or the Maillefer barrier screw (open symbols).

Steady shear flow. Figure 12 illustrates the rheological properties of the polymer melts obtained by steady-state shear rate tests, with the viscosity plotted as a function of shear rate. In this study, the measurements were restricted to rather low shear rates due to the high viscosity of the reinforced samples which generated high torques. In the measured shear rate range, the nanocellulose reinforced composites exhibited, as expected, a shear-thinning behavior. In all cases, the results of the two-pass and three-pass samples overlapped, resulting in the omission of the data from the two-pass samples in Fig. 12.

Compared to the matrix, the viscosity of the composites increased appreciably in the presence of the reinforcement with the three-pass samples showing a higher viscosity than the one-pass samples. This was most prominent with the samples based on the S1 screw configuration which showed the highest viscosity for the three-pass samples, see Fig. 12a and b. The samples shaped with the Maillefer barrier screw had a higher viscosity than the samples shaped with Maddock-type barrier screw at the first pass and displayed the steepest slope among all the samples, see Fig. 12b. The

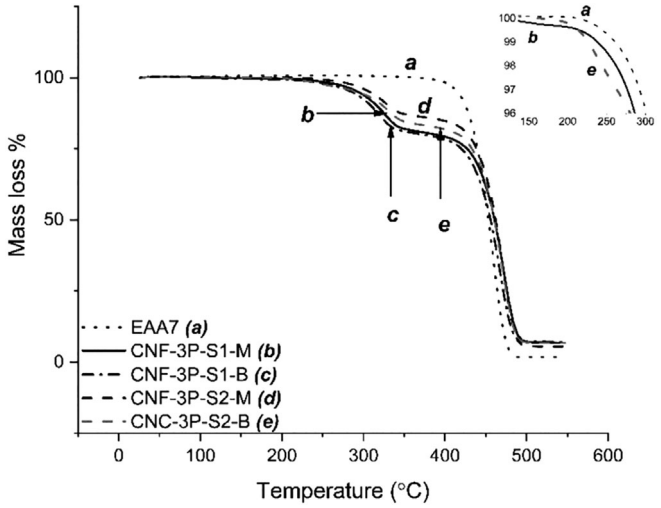

FIG. 13 Thermogravimetric curves exhibiting the degradation of the 20 vol % CNF- (b–d) and CNC-(e) reinforced composites compounded using the S1 (b and c) or S2 (d and e) screw and shaped using either the Maddock type (b and d) or Maillefer barrier screw (c and e).

CNC-containing samples showed the lowest viscosity with a small plateau in the shear thinning region around 1–3 s^{-1}, see Fig. 12a. This increase in viscosity was associated with the formation of a network of cellulosic entities which strengthened with an increasing number of passes. The plateau in the shear-thinning region for the CNC-containing samples may be related to reorientations which cause a brief increase/plateau in viscosity. This type of phenomenon has been observed in composites with a high fiber content where the orientation during shear thinning causes the reinforcements to cluster together resulting in a plateau/increase in viscosity [15].

On the other hand, the results also suggest that the Maillefer barrier screw could be a more efficient option for use in shaping which agrees with the results from the mechanical measurements. It is evident that the CNF-reinforced composites contained a more coherent network which in turn had a stronger influence on the properties of the composites.

Thermal Transitions and Crystallinity

Figure 13 shows the thermal degradation behavior of the 20 vol% nanocellulose composites together with that of the neat EAA7. It is evident that the addition of reinforcement reduces the thermal stability of the matrix by approximately 160°C, depending on the type of nanocellulose used. Since the results of the one-pass, two-pass and three-pass samples overlapped, the data from the one-pass and two-pass samples were omitted in Fig. 13. There was no difference in thermal stability between the two-pass and three-pass samples. The material compounded with the S1 screw configuration, which had the longer residence time, showed a somewhat larger mass loss than that compounded with the lower residence time screw configuration, S2, as shown in Fig. 13. The samples compounded with the S1 screw configuration showed a similar degradation behavior regardless of the screw type used during shaping, see Fig. 13. Despite being compounded using the S2 screw configuration, the CNC-containing composites showed an onset of thermal degradation at a lower temperature, 227°C, than the CNF-containing composites, 284°C,

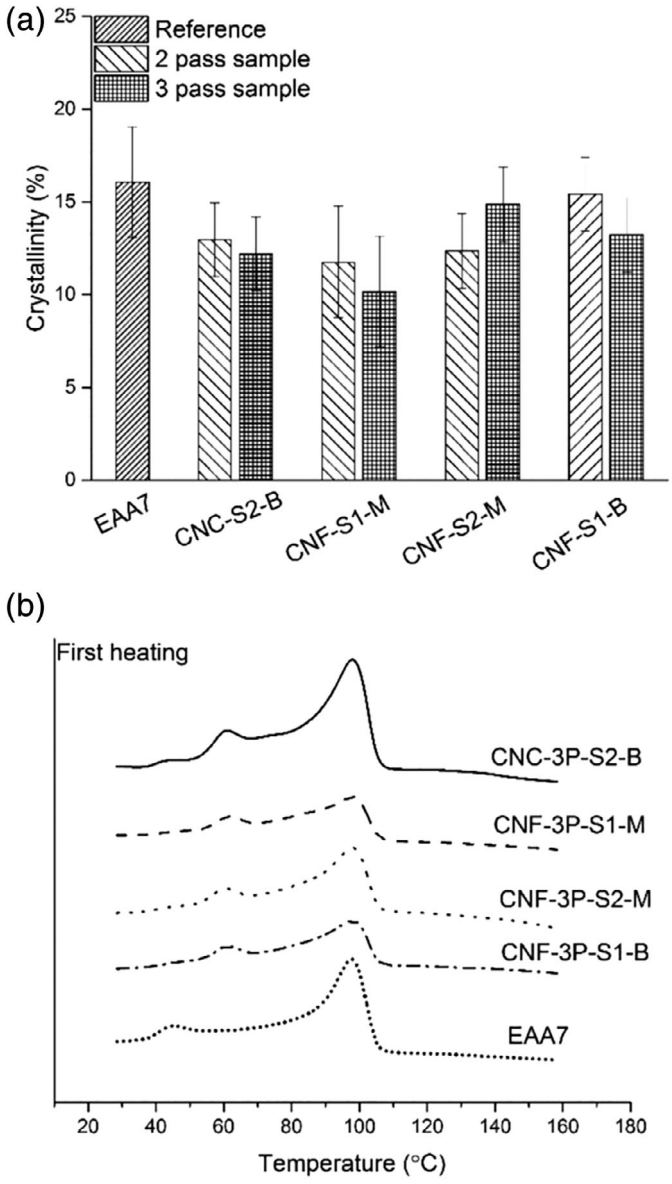

FIG. 14 (a) The crystallinity of unfilled EAA7 and nanocellulose-containing composites (b) DSC endotherms of composites reinforced with nanocellulose.

see inset plot in Fig. 13. This is also related to the relatively lower thermal stability of the sulfuric acid hydrolyzed CNC due to the presence of sulfate esters groups on their surface [9, 10]. However, the rather high thermal stability of the CNC-containing composites, in this case, could be related to the spray-dried, Na + salt neutralized CNC that was used as a starting material. The neutralized CNC had a higher thermal stability than their non-neutralized counterparts due to the reduction in the number of sulfate ester groups [9].

The addition of reinforcement to EAA7 had a negligible effect on the crystallinity of the composite, see Fig. 14a, as has been reported for other EAA-based nanocellulose composites [6, 16]. Thus, the improvement in the mechanical properties can be associated with the presence of nanocellulose reinforcements rather than with changes in the crystallinity of the composites. In Fig. 14b, the DSC thermograms show the presence of multiple endothermic peaks, which are commonly observed in ethylene-acrylic and ethylene-methacrylic acid copolymer systems, due to the melting of secondary inter-lamellar crystals. They disappear upon reheating [6, 17]. However, in this case, the lower endothermic peak has been shifted from 44°C to 60°C for the nanocellulose-reinforced samples while the larger endothermic peak at 98°C remains the same. This suggests that the reinforcements affect the size of the secondary crystallites even if their impact on overall the crystallinity is negligible.

CONCLUSIONS

The work elucidates the importance of screw configuration, type of screw, the number of passes and the morphology of reinforcement in controlling the final properties of nanocellulose-based composites. The melt processing of 20 vol% nanocellulose composites was performed by compounding a masterbatch in a twin-screw extruder followed by shaping in a single screw extruder. Two different screw configurations, S1 and S2, were used to obtain different residence times within the barrel during compounding. The pellets from the compounding step were then shaped into films with the SSE using two different barrier flank types of screws—a Maillefer barrier screw and a Maddock-type barrier screw.

Multiple passes during the compounding of the pellets were necessary to breakdown the aggregates and achieve optimum properties in the composites, despite the progressive browning of the samples. The screw configuration, which decided the residence time, determined the degree of dispersive and distributive mixing and the extent of browning of the samples. The combination of dispersive and distributive mixing was most important for obtaining the optimum properties, rather than either of them alone, as highlighted by the properties of the *CNF-S1-B* series which showed larger aggregates despite being the best composite produced. The aspect ratio of the reinforcement played an important role if the favorable choice of screw was made during shaping, as seen in the comparison between *CNF-S2-M* and *CNC-S2-B* which showed that CNC was a better reinforcement.

The presence of a nanocellulose network was further revealed through melt rheology, and the network strength increased with increasing number of passes, stabilizing after two passes suggesting the importance of multiple extrusions in improving the composite properties. It also brings into focus the reformation of a strong cellulose network despite re-extrusion. A reduction in thermal stability of the samples was observed, and the CNC-containing samples showed the lowest onset temperature for thermal degradation. The reinforcement and processing steps led to an increase in the low-temperature melting endotherm of the composites, suggesting an influence on the size of the secondary crystallites despite a negligible effect on the overall crystallinity.

ACKNOWLEDGMENTS

The authors gratefully acknowledge the funding from the Swedish Foundation for Strategic Research. Karin Sahlin-Sjövold acknowledges the Knut and Alice Wallenberg Foundation through the Wallenberg Wood Science Centre. Thanks are due to Jörgen Romild for help with the tensile testing and to Dr. J. A. Bristow for the linguistic revision of the manuscript.

REFERENCES AND CITED WORK

1. T. Saito, S. Kimura, Y. Nishiyama, and A. Isogai, *Biomacromolecules*, **8**(**8**), 2485 (2007). https://doi.org/10.1021/bm0703970.
2. L.A. Berglund and T. Peijs, *MRS Bull.*, **35**(**03**), 201 (2010). https://doi.org/10.1557/mrs2010.652.
3. K. Oksman, Y. Aitomäki, A.P. Mathew, G. Siqueira, Q. Zhou, S. Butylina, S. Tanpichai, X. Zhou, and S. Hooshmand, *Compos. Part A Appl. Sci. Manuf.*, **83**, 2 (2016). https://doi.org/10.1016/j.compositesa.2015.10.041.
4. Y. Igarashi, A. Sato, H. Okumura, F. Nakatsubo, and H. Yano, *Chem. Eng. J.*, **354**(**April**), 563 (2018). https://doi.org/10.1016/j.cej.2018.08.020.
5. K. Suzuki, H. Okumura, K. Kitagawa, S. Sato, A.N. Nakagaito, and H. Yano, *Cellulose*, **20**(**1**), 201 (2013). https://doi.org/10.1007/s10570-012-9843-9.
6. A. Venkatesh, J. Thunberg, T. Moberg, M. Klingberg, L. Hammar, A. Peterson, C. Müller, and A. Boldizar, *Cellulose*, **25**(**8**), 4577 (2018). https://doi.org/10.1007/s10570-018-1875-3.
7. R. Ariño and A. Boldizar, *Polym. Eng. Sci.*, **52**(**9**), 1951 (2012). https://doi.org/10.1002/pen.23134.
8. B. Wunderlich and C.M. Cormier, *J. Polym. Sci. Part A-2 Polym. Phys.*, **5**(**5**), 987 (1967). https://doi.org/10.1002/pol.1967.160050514.
9. M. Roman and W.T. Winter, *Biomacromolecules*, **5**(**5**), 1671 (2004). https://doi.org/10.1021/BM034519+.
10. N. Wang, E. Ding, and R. Cheng, *Polymer (Guildf).*, **48** (**12**), 3486 (2007). https://doi.org/10.1016/j.polymer.2007.03.062.
11. I. Besbes, A. Magnin, and S. Boufi, *Polym. Compos.*, **32**(**12**), 2070 (2011). https://doi.org/10.1002/pc.21232.
12. V. Khoshkava and M.R. Kamal, *ACS Appl. Mater. Interfaces*, **6** (**11**), 8146 (2014). https://doi.org/10.1021/am500577e.
13. D. Shumigin, E. Tarasova, A. Krumme, and M.P. Rheological, *Composites*, **17**(**1**), 32 (2011).
14. A. Sharif-Pakdaman, J. Morshedian, and Y. Jahani, *J. Appl. Polym. Sci.*, **125**(**S1**), E305 (2012). https://doi.org/10.1002/app.36367.
15. R. Guo, J. Azaiez, and C. Bellehumeur, *Polym. Eng. Sci.*, **45**(**3**), 385 (2005). https://doi.org/10.1002/pen.20285.
16. L. Forsgren, K. Sahlin-Sjövold, A. Venkatesh, J. Thunberg, R. Kádár, A. Boldizar, G. Westman, and M. Rigdahl, *J. Mater. Sci.*, **54**(**4**), 3009 (2019). https://doi.org/10.1007/s10853-018-3029-2.
17. K. Wakabayashi and R.A. Register, *Macromolecules*, **39**(**3**), 1079 (2006). https://doi.org/10.1021/ma052081v.